ISSN 0915-633X

INTERNATIONAL ATOMIC ENERGY AGENCY

SIXTEENTH IAEA FUSION ENERGY CONFERENCE

Montréal, Canada, 7-11 October 1996

IAEA-CN-64/C1-5

NATIONAL INSTITUTE FOR FUSION SCIENCE

An Experimental Study of Plasma Confinement and Heating Efficiency through the Potential

A. Fujisawa, S. Kubo, H. Iguchi, H. Idei, T. Minami, H. Sanuki, K. Itoh, S. Okamura, K. Matsuoka, K. Tanaka, S. Lee, M. Kojima, T.P. Crowley, Y. Hamada, M. Iwase, H. Nagasaki, H. Suzuki, N. Inoue, R. Akiyama, M. Osakabe, S. Morita, C. Takahashi, S. Muto, A. Ejiri, K. Ida, S. Nishimura, K. Narihara, I. Yamada, K. Toi, S. Ohdachi, T. Ozaki, A. Komori, K. Nishimura, S. Hidekuma, K. Ohkubo, D.A. Rasmussen, J.B. Wilgen, M. Murakami, T. Watari and M. Fujiwara

(Received - Aug. 30, 1996)

NIFS-444 Sep. 1996

RESEARCH REPORT
NIFS Series

NAGOYA, JAPAN

INTERNATIONAL ATOMIC ENERGY AGENCY

SIXTEENTH IAEA FUSION ENERGY CONFERENCE

Montréal, Canada, 7–11 October 1996

IAEA-CN-64/

An Experimental Study of Plasma Confinement and Heating Efficiency through the Potential Profile Measurements with a Heavy Ion Beam Probe in the Compact Helical System

A. Fujisawa, S. Kubo, H. Iguchi, H. Idei, T. Minami, H. Sanuki, K. Itoh, S. Okamura, K. Matsuoka, K. Tanaka, S. Lee, M. Kojima, [1]T. P. Crowley, Y. Hamada, M. Iwase, H. Nagasaki, H. Suzuki, N. Inoue, R. Akiyama, M. Osakabe, S. Morita, C. Takahashi, S. Muto, A. Ejiri, K. Ida, S. Nishimura, K. Narihara, I. Yamada, K. Toi, S. Ohdachi, T. Ozaki, A. Komori, K. Nishimura, S. Hidekuma, K. Ohkubo, [2]D. A. Rasmussen, [2]J. B. Wilgen, [2]M. Murakami, T. Watari, M. Fujiwara

National Institute for Fusion Science
Furo-cho, Chikusa-ku, Nagoya, 464-01 Japan

[1]Rensselaer Polytechnic Institute,
Troy, NY, USA 12181

[2]Oak Ridge National Laboratory,
Oak Ridge, Tennessee, USA 37831-8072

keyword: potential profile, loss cone diagram, transition, momentum transport barrier, high power ECH, high electron temperature,MHD bursts, potential profile oscillation

F1-CN-64/C1-5

An Experimental Study of Plasma Confinement and Heating Efficiency through the Potential Profile Measurements with a Heavy Ion Beam Probe in the Compact Helical System

Abstract

In the Compact Helical System (CHS), electrostatic potential profiles in steady states and transient phases of various plasmas have been measured with a 200keV heavy ion beam probe(HIBP). Potential profiles in steady states of the ECH and NBI plasmas show electron and ion root characteristics, respectively. Recent extension of the ECH system, in terms of power and controllability of focus point and polarization direction, produces a plasma with high central electron temperature of 2keV in 500kW ECH (53.2GHz) fundamental heating in 1.7T operation. A 300kW ECH heated plasma using second harmonic resonance at 0.9T has a positive profile with $\phi(0)$=400V, which exhibits a unique characteristic suggesting an internal momentum transport barrier at ρ=0.4. When the NBI is applied on this plasma, positive potential around the core region is kept for more than 10ms which is longer than the energy confinement time of a few ms, although the potential around the edge turns to be negative in about 5ms. During this phase, a dynamical behavior of potential, or transition phenomenon in a few hundred μs, is also discovered around the core. A loss cone evaluation based on the measured potential profiles gives an insight of high energy particle behaviors for both positive and negative potential profiles. A periodic change in the potential profile and internal potential fluctuation were detected in MHD bursts phenomena observed in low density NBI plasmas.

1. Introduction

The Compact Helical System (CHS)[1] is a heliotron/torsatron device which has a smaller aspect ratio of about 5; major and averaged minor radius are 1.0m, and 0.2m, respectively. Such a small aspect ratio device has a potential of higher β-limit for MHD stability, and it could be superior from an economical point of view. However, large toroidicity of such a device give birth to large deviation of ripple trapped particles from the magnetic flux surface. It will result in deterioration of confinement property and heating efficiency in a collisionless regime. Plasma potential is a key physics quantity to affect the confinement property and heating efficiency by inducing an ExB motion to the orbits of helically trapped particles.

The radial electric field of the NBI plasmas in CHS has been deduced from plasma rotation velocity measurements with a Charge Exchange Spectroscopy (CXR) system[2]. A 200keV HIBP has begun to operate to study roles of the space potential on the CHS plasma[3], and measured electrostatic potentials (or electric fields) profiles in both ECH and NBI, covering over the whole plasma region within a short period (a few ms) of a discharge. The gyrotron system has been recently enhanced to explore the plasma behavior in low collisional regime for electrons[4]. In fact, the electron temperature has been observed to be about 2keV around the core

in the 1.7T operation with fundamental resonance heating of 53.2GHz.

In this paper we will describe three main experimental topics concerning with the potential measurements; (1) potential profiles in steady state of ECH and NBI plasmas, and a unique potential profile in high power ECH operation, (2) a time evolution of potential profile and its dynamical behavior around the core while the NBI is applied on high power ECH heated plasma, (3) a DC potential oscillation and local potential fluctuation associated with the MHD dynamical evolution. The high energy particle behavior will be discussed by evaluating a loss cone structure from the obtained potential profiles.

2. Brief Description of Experimental Set-up

2-1. 200keV HIBP System

In principle of the potential measurements with the HIBPs, singly charged heavy ions (primary beam) are injected into plasmas, then doubly charged ions(secondary beam) come out from the target plasma with the energy change corresponding to the space potential at the birth point. The analyzer of HIBP is required to distinguish a few dozen volts change (potential) in several hundred kilovolts beams (primary beam energy).

In the CHS HIBP, a secondary beam sweep system is introduced in addition to the primary sweep system to manage 3-D trajectories in the toroidal helical plasmas. This method, which we call *active trajectory control*, gives the following advantages; (1) reducing the potential measurement error caused by uncertainty of beam injection angle into the energy analyzer, (2) expanding the applicable configurations and the observation regions, (3) keeping the energy analyzer away from locations where the magnetic field will disturb the determination of the beam energy.

2-2. ECH and NBI Systems

A 500 kW (106.4GHz) gyrotron has been installed for high power ECH experiments in relatively high density regime. In addition to the previous two gyrotrons with 700 kW at 53.2 GHz, the total power becomes 1200 kW as power sources. Two outputs of those three gyrotrons are selected to transmit and inject the power to the CHS. The combination of the quasi-optical transmission line and launchers enables the following unique functions: (1) highly focused elliptic Gaussian beam (2) focal position controllability by steering mirror and (3) arbitrary linear polarization controllability[4].The CHS has been equipped with co-and ctr-injected neutral beam systems whose maximum powers are 1.1MW, and 0.7MW, respectively.

3. Experimental Results

3-1. Potential Profiles in Steady States

The experiments presented here were performed on the magnetic field configuration whose axis is located on R_0=92.1cm and its strength is 0.9T. The necessary energy is 71keV for 0.9T operation when a cesium beam is used. The actual observation points are distributed along the toroidal direction, and these points in Fig. 1a are the projections obtained by tracing the magnetic field line from the

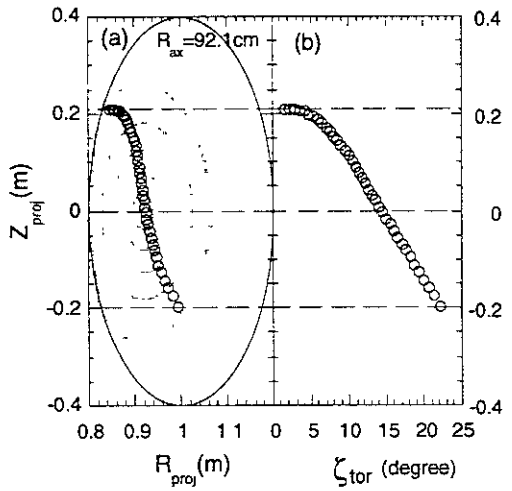

FIG. 1. (a) Projection of observation points with HIBP (b) Toroidal angle of observation points.

actual observation points. The toroidal angle ζ_{tor} of the actual observation points is also shown in Fig. 1b, where ζ_{tor} corresponds to the vertically elongated magnetic flux surface in Fig. 1a. The other configurations can be also accessed with our system, although the observation region is limited for some configurations.

Figure 2a demonstrates potential profiles obtained during steady states of ECH and NBI plasmas. The open and closed circles indicate the potential profiles of ECH plasmas with low (n_e=3x10^{12} cm^{-3}) and medium density (n_e=8x10^{12}cm^{-3}), respectively. The central electron temperatures of the low and medium density cases are $T_e(0)$=900eV, $T_e(0)$=400eV, respectively. The squares indicate the potential

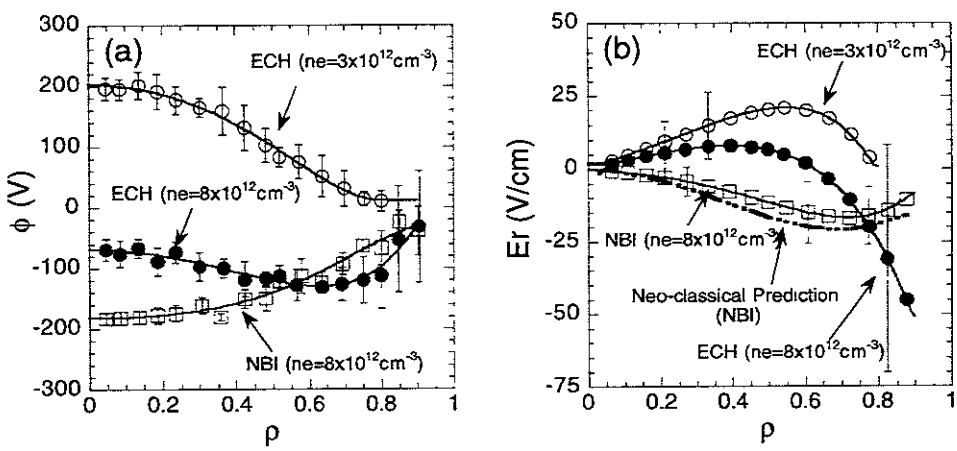

FIG. 2. (a) Potential profiles and (b) electric field profiles in steady states of ECH and NBI plasmas. The expected electric field profile from the neo-classical theory is presented by a dotted-dashed line for comparison.

profile of a co-injected NBI plasma where the electron density is $n_e=8\times10^{12}cm^{-3}$ and the electron and ion temperatures are $T_e(0)=300eV$, $T_i(0)=200eV$, respectively. The port-through NBI power was 500kW. These profiles are averages for about 20ms of steady states, and the error bars mean standard deviations.

The potential is positive with the center value of about 200 V for a low density ECH plasma with gyrotron output power of 100kW where electrons are almost in a collisionless regime since the electron collisionality is $\nu_e^*(a/2)=1.4$. The definition of the collisionality here is $\nu^*(r)=\nu_{eff}(r)/\omega_b(r)$ with $\nu_{eff}(r)=\nu(r)/\varepsilon_h$ and $\omega_b=\iota(\varepsilon_h T/m)^{1/2}/2\pi R$, where ι is the rotational transform. In the medium density ECH plasma, the potential exhibits an interesting characteristic; the electric field is positive around core, while it has a large negative value (=70V/cm) near the edge. The electron collisionality is $\nu_e^*(a/2)=13.1$, and the electron is in the plateau regime. On the other hand, the potential in the low density NBI plasma is negative with the center value of about -200 V. The collisionalities of electrons and ions are $\nu_e^*(a/2)=6.0$, $\nu_i^*(a/2)=8.2$, respectively. The electrons and ions are both in the plateau regime.

Figure 2b shows radial electric field profiles deduced from polynomial fitting curves to the obtained potential profiles. In the ECH plasmas, a tendency can be seen that the positive electric field turns more negative as the density increases. In the medium density case, the electric field shows a strong shear around the plasma edge although the statistical error bar is large. In the NBI case, the ion temperature, electron density and temperature profiles are available from the data base. Hence, the experimentally obtained electric field can be compared with the electric field predicted with the ambipolarity condition $\Gamma_i^{NC}(E_r)=\Gamma_e^{NC}(E_r)$, where $\Gamma_i^{NC}(E_r)$ and $\Gamma_e^{NC}(E_r)$ represent the electron and ion fluxes in the neoclassical theory, respectively. A dashed-dotted line in Fig. 2b represents a neoclassical prediction for the NBI plasma[5]. The theoretically expected electric field has a similar tendency to the experimental result in this case.

3-2. High Power ECH Operation and Combined Heating of ECH and NBI

The new gyrotron system can produce a plasma with the central electron temperature of 2keV with the line averaged electron density of $6\times10^{12}cm^{-3}$ when 500kW fundamental resonance heating is performed on the magnetic field configuration of $R_{ax}=92.1cm$ and 1.7T, and the microwave beam is focused on the magnetic axis. Figure 3 shows the electron temperature profile measured with a YAG Thomson scattering system whose repetition rate is 10ms. Note that negative x means the inside of the torus.

The potential profile measurements were carried out when 300kW gyrotron power was input into the magnetic field configuration of $R_{ax}=92.1cm$ and $B_0=0.9T$. Figure 4 demonstrates the obtained potential profile represented by the open circles, and the deduced electric field profile for a steady state with the line averaged electron density $n_e=3\times10^{12}cm^{-3}$. Compared to the potential profile of 100kW ECH heated plasma shown in Fig. 2a, the potential profile of 300kW exhibits a sharp peak around the core. Here, negative ρ means that the observation point is located below the magnetic axis. The existence of a sharp change in the gradient of potential (radial electric field) around $\rho=0.4$ suggests a momentum transport barrier.

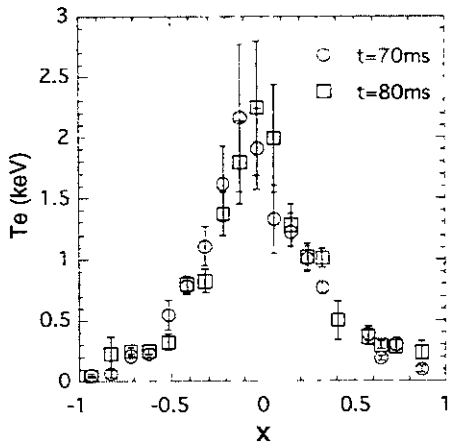

FIG. 3. Electron temperature profiles when 500kW ECH power is input to a plasma with magnetic field strength of 1.7T. The attained central temperature is about 2keV

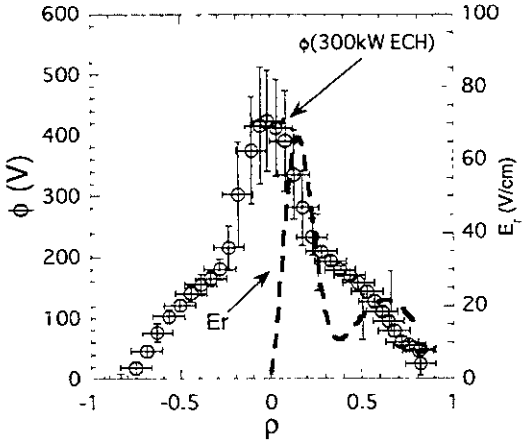

FIG.4. Potential and electric field profiles in a 300kW ECH (53.2GHz) heated plasma when the magnetic field strength is 0.9T.

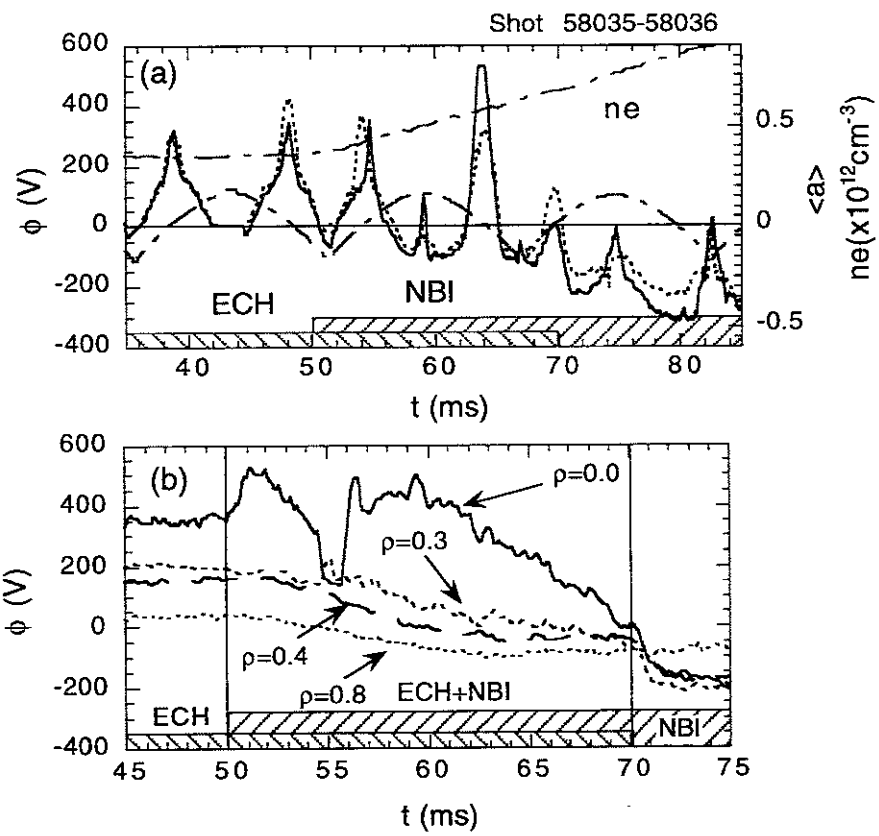

FIG. 5. (a) Potential profile evolution for ECH to NBI plasmas, together with line averaged density. The dashed-dotted line represents the averaged minor radius of the temporal observation point.(b) Time evolutions of potential at several spatial fixed points.

Figure 5a shows time evolutions of potential profiles for sequential two shots when the NBI is performed on 300kW ECH target plasmas. The port-through power of the NBI was 800kW. The dashed-dotted line indicates the averaged minor radius of the temporal observation point. Figure 5b shows the HIBP observations of time evolutions of potential at several fixed spatial points. Around the plasma core, the potential increases by $\Delta\phi(\rho=0)=200$V for 1ms just after the NBI is applied. If we estimate the full width half maximum in the time derivative of potential $d\phi/dt(\rho=0,t)$ for these changes, we obtain $\Delta T_{FWHM}=790\mu s$ at $t_0=50.3$ms by fitting a function of $(1+\gamma\exp[-\alpha(t-t_0)])^{-1}$ to the wave form in the transient phase.

And then the central potential gradually decreases and successive abrupt drop and rise by $\Delta\phi(\rho=0)=-200$V with $\Delta T_{FWHM}=150\mu s$ and $\Delta\phi(\rho=0)=400$V with $\Delta T_{FWHM}=450\mu s$ occurs at $t_0=54.5$ms, 55.9ms, respectively. This rapid structural formation around the core suggests a bifurcation of ambipolar condition $\Gamma_e(E_r)=\Gamma_i(E_r)$ since the time scale is different in the magnitude from the energy confinement time of about a few ms.

On the other hand, the potential decreases gradually at points of $\rho>0.4$. The electric field at the edge of $\rho>0.8$ turns to be negative in about 5ms from the beginning of the combined heating. In these two shots, the positive potential profiles become to be flat around nearly zero before the ECH turns off. After the ECH turns off, the central potential turns to be negative rather rapidly with $\Delta T_{FWHM}=800\mu s$, and the potential profile gradually relaxes into a steady state.

3-3. Dynamical Change of Potential Profiles Associated with MHD Bursts

Sequential periodic bursts associated with an m=2 mode have been observed with magnetic probe arrays in a low-β NBI heated plasma ($\beta=0.2\%$)[6]. Figure 6a indicates a typical example of the MHD phenomena detected with a poloidal Mirnov coil at $B_0=0.9$T, together with the toroidal beam driven current. The characteristics of these bursts are changing according to the evolution of a discharge. The expanded views for early and later stages of the discharges are shown in Figs. 6b and 6c. In the early stage, the bursts are characterized with high oscillation frequency about 40kHz to 50kHz at initial value, which decreases as a function of time. In the later stage of the discharges, the bursts are divided into two successive phases. The first phase is similar to those at the early stage of the discharge, and after this phase the bursts develop into the second phase which is characterized with low oscillation frequency about 5kHz to 10kHz, and larger amplitude in the Mirnov signals. Here, we will concentrate on the later stage of the bursts.

A poloidal array of pick-up coils shows that the wave propagation direction changes from the ion to the electron diamagnetic directions as the first phase turns to the second one. The Doppler frequency due to the plasma rotation ($=k_\theta E_r/B$) is estimated to be about 5kHz if the electric field strength is assumed to be about 30V/cm around the edge as is shown in Fig. 2b. Therefore, the change in the observed frequency should be ascribed to the propagation speed of the mode in the plasma frame. The rapid increase in the magnetic field of the second phase is also confirmed not to be caused by the plasma horizontal movement by comparing two signals from poloidal pick-up coils located on horizontally symmetrical positions.

The HIBP has found a periodic oscillation of a DC potential profile

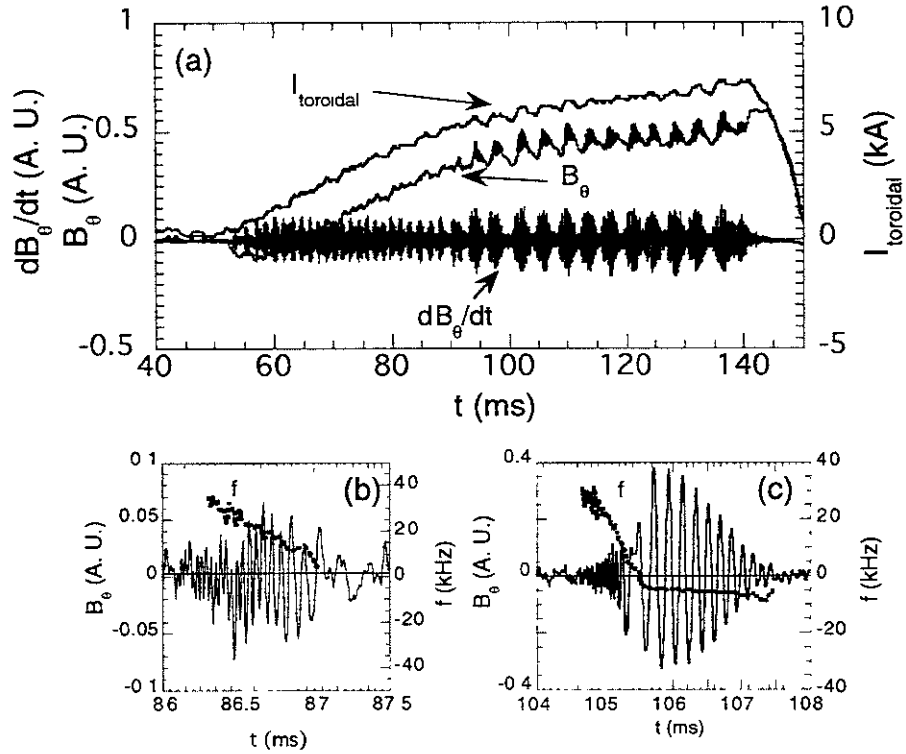

FIG. 6.(a)Overview of raw and integrated signals from a poloidal array of pick-up coils and beam driven toroidal current measured with a Rogowski coil. (b)Expanded view of bursts in the early stage of discharge, and change of its oscillation frequency (c)Expanded view of bursts in the later stage of discharge and change of its oscillation frequency.

accompanied with the evolution of the bursts in the second phase. Here, we divided the measured potential into the following two parts, $\phi = \langle\phi\rangle + \delta\phi$, where $\langle\phi\rangle$ and $\delta\phi$ are time average during 400μs (DC potential) and fluctuation part around the DC potential. Figure 7a shows the DC potential changes at several spatial points during a cycle of the bursts. The DC potential profile is not changing during the first phase of the bursts. On the other hand, Figs. 7b demonstrate that in the second phase the potential reaches its shallowest value as the magnetic field fluctuation takes its maximum. Namely, the rotation speed of plasma becomes slower. Then the potential profile becomes deeper again as the mode becomes stabilized. The recovery of the potential at the edge seems to be delayed to the central potential in a few hundred μs, however, detail spatial and temporal structure of the potential oscillation needs further observations. The relative potential variation seen in this oscillation is about 40V at the center. The occurrence of this instability is anticipated to deteriorate confinement properties. In fact, the angular momentum change in the plasma accompanied with this potential profile oscillation, is roughly estimated to be about 5×10^{-7}Nmsec, in other words, the plasma loses electric charge of about 4×10^{-5}C in a cycle[7].

Moreover, the internal structure of this mode can be inferred from fluctuation part of the potential. Figure 7c shows that the potential fluctuation is well correlated with the magnetic field fluctuation in the first phase. When it becomes closer to the second phase, the potential fluctuation becomes smaller and finally disappears in the

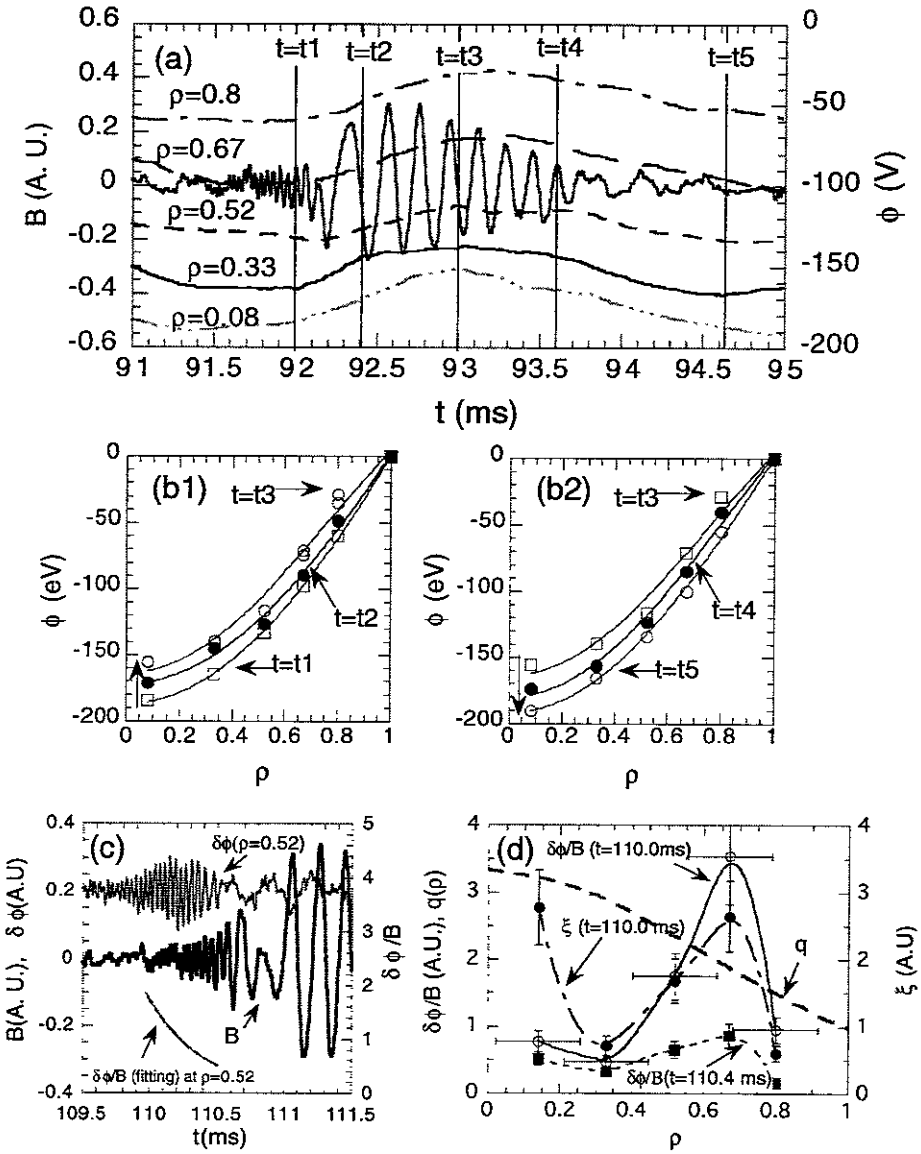

FIG. 7. (a)DC potential changes at several spatial points, accompanied with the growth of magnetic field fluctuation amplitude in the second phase of the bursts in the later stage of discharges (b1) Change of DC potential profiles in increasing phase of magnetic fluctuation amplitude (b2) Change of DC potential profiles in decreasing phase of magnetic fluctuation amplitude (c) Correlation of potential fluctuation with magnetic field fluctuation.(d) Spatial dependence of the ratio of potential fluctuation amplitude to magnetic field fluctuation amplitude, together with the q-profile. A parameter proportinal to plasma displacement ξ is also indicated in a dashed-dotted line.

second phase, and this is valid within the observation point of $\rho<0.8$. Figure 7d indicates the potential fluctuation amplitude normalized by magnetic fluctuation amplitude, together with another potential fluctuation normalized by a product of the magnetic fluctuation amplitude and electric field strength which is assumed to be E_r=-30ρ(V/cm). The definition of the latter is explicitly written as $\xi=\delta\phi/BE_r$, and the parameter ξ is proportional to the plasma displacement under the assumption that potential should be constant on the magnetic flux surface. This result implies that the mode in the first phase is dominant in the plasma inside ($\rho<0.8$).

Contrarily, in the second phase we have not observed a coherent potential fluctuation with the Mirnov coil signals at a position of $\rho<0.8$. And the total intensity of the secondary beam, which suffers from path integral effects[8], shows fluctuation synchronized with the magnetic field fluctuation. As is shown in Fig. 7d, the q-value of the vacuum field at the plasma edge is slightly below 1, and the NBI driven current flows in the direction to make the q(a) smaller. These facts suggest that the mode in the second phase should be localized in a plasma edge of $\rho>0.8$, and the evolution of the first and the second phases should be originated from different modes. Switching process between two different modes may occur at the turning point from the first phase to the second one. The information of the plasma inside, as the HIBP presented, is essential to identify the instabilities to cause the bursts which will limit plasma performance.

4. Behaviors of High Energy Particles in Loss Cone Diagrams

The loss cone structure can be easily estimated from obtained potential profiles by use of an analytic formula. According to Ref. [9], the loss cone for deeply trapped particles is expressed as $W_m<W<W_p$, where W is the particle energy, and $W_m=-q\phi(0)f(x)/(\varepsilon_{ha}(1-x^2)+\varepsilon_{ta}(1-x))$, $W_p=-q\phi(0)f(x)/(\varepsilon_{ha}(1-x^2)-\varepsilon_{ta}(1+x))$. Here, ε_{ta} and ε_{ha} represent toroidal and helical ripple coefficients, respectively, and x indicates the horizontal coordinate whose origin is on the magnetic axis, and f(x) is a normalized function fitted to the experimental profiles with f(0)=1, f(1)=f(-1)=0. For the magnetic field configuration with R_{ax}=92.1cm, we choose ε_{ta}=0.16 and ε_{ha}=0.255.

A loss cone diagram for the NBI plasma is demonstrated in Fig. 8a. The loss cone plays a role in a collisionless regime when the helically trapped particles can accomplish their one-turn orbits poloidally without a collision. This criterion is roughly expressed as $\omega_{gradB}>\nu/\varepsilon_h$. Figure 8a plots the critical energy W_{rot} to satisfy the criterion which is explicitly written as $W_{rot}{}^{2.5}(eV)>1.4\times10^{-2}n_e(cm^{-3})B(T)r(cm)^2\varepsilon_h^{-2}$. This criterion is no longer valid around the magnetic axis since there the banana width is larger than the local structure owing to the small poloidal field.

When the NBI is injected into this plasma, the energy transfer rates to ions and electrons are a function of electron temperature. The beam energy to heat ions and electrons equally is represented by $W_{pi=pe}=15T_eA_b[Z_i^2/A_i]^{2/3}$, where A_b, A_i and Z_i are the atomic mass of the beam particles, the atomic mass and the charge of the bulk plasmas, respectively. Above this energy (=$15T_e$), the beam particles heat selectively electrons, preserving the pitch angle. On the other hand, the injected beam particles experience pitch angle scatterings in the region below this energy, and simultaneously the beam particles transfer their energy to ions. It becomes, therefore, more probable for the beam particles to enter into the loss cone below this energy.

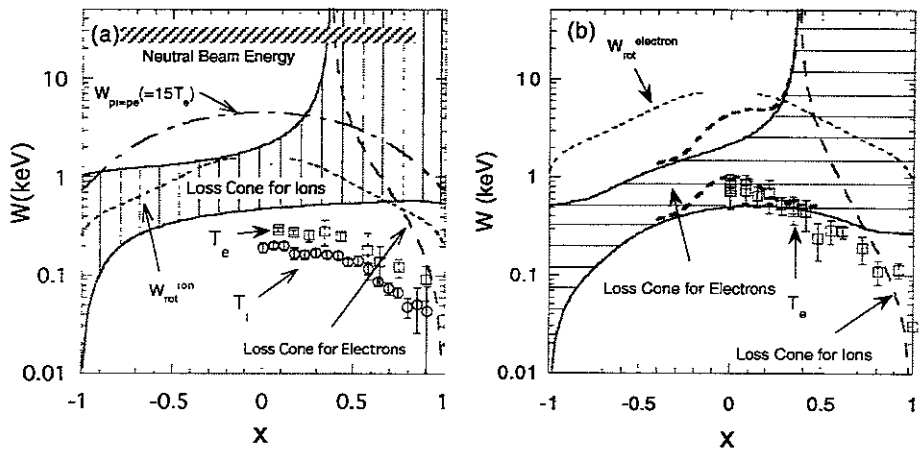

FIG. 8. (a)Loss cone diagrams for deeply trapped ions in the NBI plasmas with $\phi(0)$=-200V. The dashed line shows loss cone boundary for deeply trapped electrons. (b) Loss cone diagrams for deeply trapped electrons in ECH plasma with $\phi(0)$=200V. The dashed line shows loss cone boundary for deeply trapped ions. The longer dashed line represents the loss cone boundary for electrons in 300kW ECH heated plasmas. The loss cone plays a role in the region above the dashed line W_{rot}. This line means the particle (ion or electron) energy at which the particle can accomplish poloidally one-turn orbits.

The neutral beam is tangentially injected in the CHS with the energy about 38 keV (the hatched region in Fig. 8a). The effective energy transfer from injected beams to bulk ions occurs in the regime between the upper loss cone boundary and the energy of $W_{pi=pe}(=15T_e)$. As for the bulk ions, the temperature is below the lower loss cone boundary. Hence, the bulk ions are confined by the rotation due to ExB motion. If the potential becomes sufficiently negative for the loss cone region to be located above the energy of $W_{pi=pe}$, the ion heating efficiency will be improved since the pitch angle scatterings occur below the loss cone region.The dashed line in the figure shows the loss cone for electrons in the NBI plasma.

A loss cone diagram for deeply trapped electrons can be also demonstrated for the low density ECH plasma with a positive potential shown in Fig. 8b. It is shown in Fig. 8b that the loss cone region above the energy of W_{rot} exists only in the outside (x>0). The critical energy W_{rot} for electrons is higher than that for ions since the collision frequency is larger for the same energy; $W_{rot}^{2.5}(eV)>6.3\times10^{-1}n_e(cm^{-3})B(T)r(cm)^2\varepsilon_h^{-2}$. Thus, the electron heated up by the wave on the outside of torus will easily enter into the loss cone. In case of the potential profile of the 300kW ECH heated plasma, the loss cone boundary around the core region moves toward high energy side as is indicated by a longer dashed line. As for ions, the loss cone region in this positive potential is localized only in an outside periphery of the plasma. The loss cone boundary for ions is shown by the dashed line in Fig.8b. Therefore, highly effective heating due to high energy ions are expected in the plasmas with positive potential.

As is shown in Fig.4, a positive potential was observed to be maintained for

a longer time than the energy confinement time except the edge region during a combined heating phase of the NBI and ECH, although the positive potential tends to become negative gradually before the ECH off. In the phase of positive potential, it is expected that the deposited high energy particles of NBI may be well confined in the plasma and these high energy particles may heat the bulk plasma effectively. It was observed that in some shots positive potential was held for about 20ms until ECH turns off. The mechanism of potential generation need further investigation to realize high heating efficiency and confinement of the toroidal helical plasmas.

5. Summary

In summary, we have obtained the following results in CHS after a new ECH and a 200keV HIBP system started to operate. (1)High electron temperature about 2keV was achieved at the first time when fundamental 500kW heating was performed at B_0=1.7T. (2)Steady state potential profiles varied widely between NBI and ECH heated plasmas which show negative and positive profiles, respectively, and loss cone diagrams were evaluated using the obtained potential profiles to discuss the behavior of high energy particles. (3)A unique potential profile suggesting existence of a momentum transport barrier was found around the core when 300kW ECH heating was performed at B_0=0.9T. (4)A transition phenomenon in electric field, suggesting a bifurcation of solutions in the ambipolar condition, was observed around the plasma core during the combined heating phase of the NBI and ECH. (5) Internal structure of the MHD bursts, which may deteriorate confinement properties, was investigated through the potential profile and its fluctuation measurements. The HIBP is a powerful tool to study the physics of toroidal helical plasmas through static and dynamic behaviors in potential, and to give a better understanding of heating efficiency and confinement.

References

[1]MATSUOKA, K., et al., in Plasma Phys. and Controll. Nuclear Fusion Research, 1988 Nice (IEAE, Vienna, 1989), Vol. **11**, p411.
[2] IDA, K., et al., Phys. Fluids B **3**, (1991)5151.
[3] FUJISAWA, A., et al., Rev. Sci. Instrum. **63** (1992)3694.
[4] KUBO, S., et al., Fusion Eng. and Design **26** (1994)319.
[5]SANUKI, H., et al., J. of Phys. Soc. Jpn. **62** (1993)123.
[6]SAKAKIBARA, S., et al., J. of Phys. Soc. Jpn, **63** (1994)4406.
[7]ITOH, K. et al., , Plasma Phys. Control. Fusion **38** (1996)1.
[8]ROSS, D., et al., Nucl. Fusion **36** (1991)1355.
[9] ITOH, K., et al., Phys. Fluids B **3** (1991)1294.

Recent Issues of NIFS Series

NIFS-406 M. Tanaka and D. Biskamp,
Symmetry-Breaking due to Parallel Electron Motion and Resultant Scaling in Collisionless Magnetic Reconnection; Mar. 1996

NIFS-407 K. Kitachi, T. Oike, S. Ohdachi, K. Toi, R. Akiyama, A. Ejiri, Y. Hamada, H.Kuramoto, K. Narihara, T. Seki and JIPP T-IIU Group,
Measurement of Magnetic Field Fluctuations within Last Closed Flux Surface with Movable Magnetic Probe Array in the JIPP T-IIU Tokamak; Mar. 1996

NIFS-408 K. Hirose, S. Saito and Yoshi.H. Ichikawa
Structure of Period-2 Step-1 Accelerator Island in Area Preserving Maps; Mar. 1996

NIFS-409 G.Y.Yu, M. Okamoto, H. Sanuki, T. Amano,
Effect of Plasma Inertia on Vertical Displacement Instability in Tokamaks; Mar. 1996

NIFS-410 T. Yamagishi,
Solution of Initial Value Problem of Gyro-Kinetic Equation; Mar. 1996

NIFS-411 K. Ida and N. Nakajima,
Comparison of Parallel Viscosity with Neoclassical Theory; Apr. 1996

NIFS-412 T. Ohkawa and H. Ohkawa,
Cuspher, A Combined Confinement System; Apr. 1996

NIFS-413 Y. Nomura, Y.H. Ichikawa and A.T. Filippov,
Stochasticity in the Josephson Map; Apr. 1996

NIFS-414 J. Uramoto,
Production Mechanism of Negative Pionlike Particles in H_2 Gas Discharge Plasma; Apr. 1996

NIFS-415 A. Fujisawa, H. Iguchi, S. Lee, T.P. Crowley, Y. Hamada, S. Hidekuma, M. Kojima,
Active Trajectory Control for a Heavy Ion Beam Probe on the Compact Helical System; May 1996

NIFS-416 M. Iwase, K. Ohkubo, S. Kubo and H. Idei
Band Rejection Filter for Measurement of Electron Cyclotron Emission during Electron Cyclotron Heating; May 1996

NIFS-417 T. Yabe, H. Daido,T. Aoki, E. Matsunaga and K. Arisawa,
Anomalous Crater Formation in Pulsed-Laser-Illuminated Aluminum Slab and Debris Distribution; May 1996

NIFS-418 J. Uramoto,
Extraction of K^- Mesonlike Particles from a D_2 Gas Discharge Plasma in Magnetic Field; May 1996

NIFS-419 J. Xu, K. Toi, H. Kuramoto, A. Nishizawa, J. Fujita, A. Ejiri, K. Narihara, T. Seki, H. Sakakita, K. Kawahata, K. Ida, K. Adachi, R. Akiyama, Y. Hamada, S. Hirokura, Y. Kawasumi, M. Kojima, I. Nomura, S. Ohdachi, K.N. Sato
Measurement of Internal Magnetic Field with Motional Stark Polarimetry in Current Ramp-Up Experiments of JIPP T-IIU; June 1996

NIFS-420 Y.N. Nejoh,
Arbitrary Amplitude Ion-acoustic Waves in a Relativistic Electron-beam Plasma System; July 1996

NIFS-421 K. Kondo, K. Ida, C. Christou, V.Yu.Sergeev, K.V.Khlopenkov, S.Sudo, F. Sano, H. Zushi, T. Mizuuchi, S. Besshou, H. Okada, K. Nagasaki, K. Sakamoto, Y. Kurimoto, H. Funaba, T. Hamada, T. Kinoshita, S. Kado, Y. Kanda, T. Okamoto, M. Wakatani and T. Obiki,
Behavior of Pellet Injected Li Ions into Heliotron E Plasmas; July 1996

NIFS-422 Y. Kondoh, M. Yamaguchi and K. Yokozuka,
Simulations of Toroidal Current Drive without External Magnetic Helicity Injection; July 1996

NIFS-423 Joong-San Koog,
Development of an Imaging VUV Monochromator in Normal Incidence Region; July 1996

NIFS-424 K. Orito,
A New Technique Based on the Transformation of Variables for Nonlinear Drift and Rossby Vortices; July 1996

NIFS-425 A. Fujisawa, H. Iguchi, S. Lee, T.P. Crowley, Y. Hamada, H. Sanuki, K. Itoh, S. Kubo, H. Idei, T. Minami, K. Tanaka, K. Ida, S. Nishimura, S. Hidekuma, M. Kojima, C. Takahashi, S. Okamura and K. Matsuoka,
Direct Observation of Potential Profiles with a 200keV Heavy Ion Beam Probe and Evaluation of Loss Cone Structure in Toroidal Helical Plasmas on the Compact Helical System; July 1996

NIFS-426 H. Kitauchi, K. Araki and S. Kida,
Flow Structure of Thermal Convection in a Rotating Spherical Shell; July 1996

NIFS-427 S. Kida and S. Goto,
Lagrangian Direct-interaction Approximation for Homogeneous Isotropic Turbulence; July 1996

NIFS-428 V.Yu. Sergeev, K.V. Khlopenkov, B.V. Kuteev, S. Sudo, K. Kondo, F. Sano, H. Zushi, H. Okada, S. Besshou, T. Mizuuchi, K Nagasaki, Y Kurimoto and T. Obiki,
Recent Experiments on Li Pellet Injection into Heliotron E; Aug. 1996

NIFS-429 N. Noda, V. Philipps and R. Neu,
A Review of Recent Experiments on W and High Z Materials as Plasma-Facing Components in Magnetic Fusion Devices; Aug. 1996

NIFS-430 R.L. Tobler, A. Nishimura and J. Yamamoto,
Design-Relevant Mechanical Properties of 316-Type Stainless Steels for Superconducting Magnets; Aug. 1996

NIFS-431 K. Tsuzuki, M. Natsir, N. Inoue, A. Sagara, N. Noda, O. Motojima, T. Mochizuki, T. Hino and T. Yamashina,
Hydrogen Absorption Behavior into Boron Films by Glow Discharges in Hydrogen and Helium; Aug. 1996

NIFS-432 T.-H. Watanabe, T. Sato and T. Hayashi,
Magnetohydrodynamic Simulation on Co- and Counter-helicity Merging of Spheromaks and Driven Magnetic Reconnection; Aug. 1996

NIFS-433 R. Horiuchi and T. Sato,
Particle Simulation Study of Collisionless Driven Reconnection in a Sheared Magnetic Field; Aug. 1996

NIFS-434 Y. Suzuki, K. Kusano and K. Nishikawa,
Three-Dimensional Simulation Study of the Magnetohydrodynamic Relaxation Process in the Solar Corona. II.; Aug. 1996

NIFS-435 H. Sugama and W. Horton,
Transport Processes and Entropy Production in Toroidally Rotating Plasmas with Electrostatic Turbulence; Aug. 1996

NIFS-436 T. Kato, E. Rachlew-Källne, P. Hörling and K.-D Zastrow,
Observations and Modelling of Line Intensity Ratios of OV Multiplet Lines for 2s3s 3S1 - 2s3p 3Pj; Aug. 1996

NIFS-437 T. Morisaki, A. Komori, R. Akiyama, H. Idei, H. Iguchi, N. Inoue, Y. Kawai, S. Kubo, S. Masuzaki, K. Matsuoka, T. Minami, S. Morita, N. Noda, N. Ohyabu, S. Okamura, M. Osakabe, H. Suzuki, K. Tanaka, C. Takahashi, H. Yamada, I. Yamada and O. Motojima,
Experimental Study of Edge Plasma Structure in Various Discharges on Compact Helical System; Aug. 1996

NIFS-438 A. Komori, N. Ohyabu, S. Masuzaki, T. Morisaki, H. Suzuki, C. Takahashi, S. Sakakibara, K. Watanabe, T. Watanabe, T. Minami, S. Morita, K. Tanaka, S. Ohdachi, S. Kubo, N. Inoue, H. Yamada, K. Nishimura, S. Okamura, K. Matsuoka, O. Motojima, M. Fujiwara, A. Iiyoshi, C. C. Klepper, J.F. Lyon, A.C.

England, D.E. Greenwood, D.K. Lee, D.R. Overbey, J.A. Rome, D.E. Schechter and C.T. Wilson,
Edge Plasma Control by a Local Island Divertor in the Compact Helical System; Sep. 1996 (IAEA-CN-64/C1-2)

NIFS-439 K. Ida, K. Kondo, K. Nagaski T. Hamada, H. Zushi, S. Hidekuma, F. Sano, T. Mizuuchi, H. Okada, S. Besshou, H. Funaba, Y. Kurimoto, K. Watanabe and T. Obiki,
Dynamics of Ion Temperature in Heliotron-E; Sep. 1996 (IAEA-CN-64/CP-5)

NIFS-440 S. Morita, H. Idei, H. Iguchi, S. Kubo, K. Matsuoka, T. Minami, S. Okamura, T. Ozaki, K. Tanaka, K. Toi, R. Akiyama, A. Ejiri, A. Fujisawa, M. Fujiwara, M. Goto, K. Ida, N. Inoue, A. Komori, R. Kumazawa, S. Masuzaki, T. Morisaki, S. Muto, K. Narihara, K. Nishimura, I. Nomura, S. Ohdachi, M.. Osakabe, A. Sagara, Y. Shirai, H. Suzuki, C. Takahashi, K. Tsumori, T. Watari, H. Yamada and I. Yamada,
A Study on Density Profile and Density Limit of NBI Plasmas in CHS; Sep. 1996 (IAEA-CN-64/CP-3)

NIFS-441 O. Kaneko, Y. Takeiri, K. Tsumori, Y. Oka, M. Osakabe, R. Akiyama, T. Kawamoto, E. Asano and T. Kuroda,
Development of Negative-Ion-Based Neutral Beam Injector for the Large Helical Device; Sep. 1996 (IAEA-CN-64/GP-9)

NIFS-442 K. Toi, K.N. Sato, Y. Hamada, S. Ohdachi, H. Sakakita, A. Nishizawa, A. Ejiri, K. Narihara, H. Kuramoto, Y. Kawasumi, S. Kubo, T. Seki, K. Kitachi, J. Xu, K. Ida, K. Kawahata, I. Nomura, K. Adachi, R. Akiyama, A. Fujisawa, J. Fujita, N. Hiraki, S. Hidekuma, S. Hirokura, H. Idei, T. Ido, H. Iguchi, K. Iwasaki, M. Isobe, O. Kaneko, Y. Kano, M. Kojima, J. Koog, R. Kumazawa, T. Kuroda, J. Li, R. Liang, T. Minami, S. Morita, K. Ohkubo, Y. Oka, S. Okajima, M. Osakabe, Y. Sakawa, M. Sasao, K. Sato, T. Shimpo, T. Shoji, H. Sugai, T. Watari, I. Yamada and K. Yamauti,
Studies of Perturbative Plasma Transport, Ice Pellet Ablation and Sawtooth Phenomena in the JIPP T-IIU Tokamak; Sep. 1996 (IAEA-CN-64/A6-5)

NIFS-443 Y. Todo, T. Sato and The Complexity Simulation Group,
Vlasov-MHD and Particle-MHD Simulations of the Toroidal Alfvén Eigenmode; Sep. 1996 (IAEA-CN-64/D2-3)

NIFS-444 A. Fujisawa, S. Kubo, H. Iguchi, H. Idei, T. Minami, H. Sanuki, K. Itoh, S. Okamura, K. Matsuoka, K. Tanaka, S. Lee, M. Kojima, T.P. Crowley, Y. Hamada, M. Iwase, H. Nagasaki, H. Suzuki, N. Inoue, R. Akiyama, M. Osakabe, S. Morita, C. Takahashi, S. Muto, A. Ejiri, K. Ida, S. Nishimura, K. Narihara, I. Yamada, K. Toi, S. Ohdachi, T. Ozaki, A. Komori, K. Nishimura, S. Hidekuma, K. Ohkubo, D.A. Rasmussen, J.B. Wilgen, M. Murakami, T. Watari and M. Fujiwara,
An Experimental Study of Plasma Confinement and Heating Efficiency through the Potential Profile Measurements with a Heavy Ion Beam Probe in the Compact Helical System; Sep. 1996 (IAEA-CN-64/C1-5)